Chemical Science

ROYAL SOCIETY OF CHEMISTRY

EDGE ARTICLE

View Article Online
View Journal | View Issue

Cite this: *Chem. Sci.*, 2021, **12**, 9333

All publication charges for this article have been paid for by the Royal Society of Chemistry

Received 10th March 2021
Accepted 2nd June 2021

DOI: 10.1039/d1sc01401c

rsc.li/chemical-science

[GaF(H$_2$O)][IO$_3$F]: a promising NLO material obtained by anisotropic polycation substitution†

Qian-Ming Huang,[ab] Chun-Li Hu,[a] Bing-Ping Yang,*[a] Zhi Fang,[a] Yuan Lin,[a] Jin Chen,[ab] Bing-Xuan Li[a] and Jiang-Gao Mao*[ab]

A novel salt-inclusion fluoroiodate [GaF(H$_2$O)][IO$_3$F] derived from CsIO$_2$F$_2$ was ingeniously obtained through anisotropic polycation substitution. Because the catenulate [GaF(H$_2$O)]$^{2+}$ framework serves as a template for the favorable assembly of the polar [IO$_3$F]$^{2-}$ groups and contributes to the nonlinear coefficient, [GaF(H$_2$O)][IO$_3$F] exhibits a greatly improved second-harmonic generation (SHG) effect of 10 times that of KH$_2$PO$_4$ (KDP) and a considerable band gap of 4.34 eV compared to the parent compound CsIO$_2$F$_2$ (3 × KDP, 4.5 eV). Particularly, to the best of our knowledge, [GaF(H$_2$O)][IO$_3$F] has the largest laser-induced damage threshold (LDT) of 140 × AgGgS$_2$ of the reported iodates. All these results signify that [GaF(H$_2$O)][IO$_3$F] is a promising nonlinear optical (NLO) crystal. This work also proposes that anisotropic polycation substitution is an effective approach to optimize the SHG effect and develop excellent NLO materials.

Introduction

Nonlinear optical (NLO) materials are of great interest owing to their irreplaceable frequency conversion capability in all-solid-state laser technology.[1–10] Because of the absence of the lasers emitting mid-infrared (IR) (3–12 μm) light that has great advantages in the fields of spectroscopy analysis, laser surgery, laser communications, *etc.*, NLO materials used for mid-IR generation are increasingly attractive.[11–13] However, currently commercialized mid-IR NLO crystals, such as AgGaS$_2$ (AGS), AgGaSe$_2$ and ZnGeP$_2$,[14–16] have been heavily restricted by their relatively smaller band gaps which can always result in harmful two-photon absorptions and lower laser-induced damage thresholds (LDTs).[6,17–20] Consequently, it is still urgent to explore mid-IR NLO material with improved band gap (or LDT) and great comprehensive properties.

Metal iodates with the stereo-chemically active lone-electron pair (SALP) have long been investigated for mid-IR NLO applications.[21–27] Generally, incorporating asymmetric IO$_3$/IO$_4$ units with octahedrally coordinated d^0 transition-metal (TM) cations (V^{5+} and Mo^{6+}, *etc.*) and SALP-involving metal cations (Pb^{2+} and Bi^{3+}, *etc.*) can easily induce non-centrosymmetric (NCS) structures and large SHG responses,[28–36] such as BiOIO$_3$ (12.5 × KDP).[37] Nevertheless, the adoption of d^0-TM/SALP-involving metal cations would inevitably narrow the band gap due to the d–d/s–p electronic transition, and further reduce the LDT of the materials.[8,38–41] Lots of investigations have proposed that the introduction of the most electronegative fluorine anion is an effective way to enhance the band gap of iodates.[12,41–45] In the reported NCS fluorine iodates, the band gaps of iodate fluorides are still seriously limited by d^0-TM/SALP-involving cations although F$^-$ plays a positive role in improving them, such as α-Ba$_2$[VO$_2$F$_2$(IO$_3$)$_2$]IO$_3$ (9 × KDP, 2.55 eV);[46] in contrast, fluoroiodates exhibit increased band gaps (>4.2 eV) owing to the larger bond-energy sum of IO$_x$F$_y$ than IO$_3$ unit (Table S1†). However, the SHG signals of fluoroiodates deserve further enhancements mainly because of the unfavorable arrangement modes and the inherent polarity of the IO$_x$F$_y$ units, such as CsIO$_2$F$_2$ (3 × KDP, 4.5 eV).[44] Therefore, it is an ideal route to obtain exceptional mid-IR NLO crystals through increasing the nonlinear coefficient of fluoroiodates.

Recently, introducing ionic halide-salt into the chalcogenide system to form salt-inclusion structures has emerged as a new method to regulate SHG–band gap relationships of chalcogenides.[47–52] Salt-inclusion chalcogenides with mixed framework and filler can ingeniously inherit the wide band gap of halides and intense SHG effect of chalcogenides, such as Li[LiCs$_2$Cl][Ga$_3$S$_6$].[53] Inspired by the unique host–guest framework structure, in this work, the mono-atomic Cs$^+$ of CsIO$_2$F$_2$ was substituted by more anisotropic halide-salt polycation [GaF(H$_2$O)]$^{2+}$, and the [IO$_2$F$_2$]$^-$ unit also accordingly adjusted to its isomorphic [IO$_3$F]$^{2-}$; thus, a novel salt-inclusion fluoroiodate [GaF(H$_2$O)][IO$_3$F] was successfully obtained. Catenulate [GaF(H$_2$O)]$^{2+}$ framework serves as a template to regulate the arrangement of the polar [IO$_3$F]$^{2-}$ groups, resulting in an

[a]*State Key Laboratory of Structural Chemistry, Fujian Institute of Research on the Structure of Matter, Chinese Academy of Sciences, Fuzhou 350002, P. R. China. E-mail: ybp@fjirsm.ac.cn; mjg@fjirsm.ac.cn*

[b]*University of Chinese Academy of Sciences, Beijing, 100049, China*

† Electronic supplementary information (ESI) available. CCDC 2083798. For ESI and crystallographic data in CIF or other electronic format see DOI: 10.1039/d1sc01401c

unique NCS structure of $[GaF(H_2O)][IO_3F]$. Through this anisotropic polycation substitution, the SHG effect of $[GaF(H_2O)][IO_3F]$ is greatly improved (10 × KDP) while the band gap remains elevated status (4.34 eV) compared to the parent compound $CsIO_2F_2$ (3 × KDP, 4.5 eV). Herein, we report its synthesis, crystal structure, physicochemical properties and first-principle studies.

Results and discussion

$[GaF(H_2O)][IO_3F]$ single crystals were synthesized by hydrothermal method with the Ga : I ratio of 1 : 1 in HF aqueous solution (40%, highly corrosive! personal protective equipment is required, and HF should always be handled inside of a fume hood), similar to that of $CsIO_2F_2$ (ESI†). Powder X-ray diffraction (PXRD) was performed to verify the purity of the product (Fig. S1†), and the existence of Ga, F, and I was also verified by energy-dispersive X-ray spectroscopy (EDS) (Fig. S2†). The thermogravimetric analysis (TGA) of $[GaF(H_2O)][IO_3F]$ indicates that the sample has a high thermal stability up to 300 °C (Fig. S3†). Each molecule releases 0.5 I_2, 0.75 O_2, 1 H_2O and 1 F_2 during the decomposition and the measured value of weight loss (68.39%) is consistent with the calculated value (68.83%).

$[GaF(H_2O)][IO_3F]$ crystallizes in the orthogonal polar space group $Pca2_1$ (no. 29). The asymmetric unit contains 1 Ga, 1 I, 4 O, 2 F, and 2 H atoms (Fig. S4a†). The I atom is disordered over two sites (85.8% for I(1A) and 14.2% for I(1B)) and is tetrahedrally coordinated by three oxygen and one fluorine atoms, constructing a mono-fluorinated $[IO_3F]^{2-}$ anion (Fig. S4a†). The bond lengths of I(1B)–F(1) is 1.98(4) Å, which is slightly longer than I–O bonds (1.778(8)–1.858(9) Å). The I(1A) component with the major occupancy is assumed to be the only I atom in the overall structural descriptions. The Ga atom adopts the typical sixfold octahedral coordination to three O and three F atoms with Ga–O bond lengths ranging from 1.896(7) to 1.958(8) Å and Ga–F bond lengths varying from 1.860(8) to 1.933(6) Å (Fig. S4b†). The bond length differences of these six Ga–O/F bonds are very small, leading to a slightly distorted GaO_3F_3 octahedron. These coordination geometries are comparable to those of the reported iodates.[45,54,55] The calculated bond valence sum (BVS) of Ga (3.15), I (4.97), O (1.8–2.24) and F (0.79–0.88) are reasonable except the terminal atom O(4) (0.54) (Table S3†).[56] Therefore, the O(4) atom bonds to two H atoms, which constitutes the coordinating H_2O. Owing to the disordered I(1) atom, determining which atom is O and which is F is rather complicated, which is provided in ESI in detail.† The physical techniques used to characterize the material are discussed in the experimental section.

$[GaF(H_2O)][IO_3F]$ is characterized by a typical salt-inclusion structure with $[GaF(H_2O)]^{2+}$ polycation framework and assembled $[IO_3F]^{2-}$ functional building blocks. Each $GaF(H_2O)$ unit shares the F(2) atom to build a one-dimensional (1D) zigzag $[GaF(H_2O)]^{2+}$ chain along the *c* axis (Fig. 1c), and parallel $[GaF(H_2O)]^{2+}$ chains further interact with IO_3F units through O(2), O(3), and F(1) atoms, forming a 2D $[GaF(H_2O)(IO_3F)]_\infty$ layer on the *bc* plane (Fig. 1d). These $[GaF(H_2O)(IO_3F)]_\infty$ layers in two different orientations are alternately arranged in an

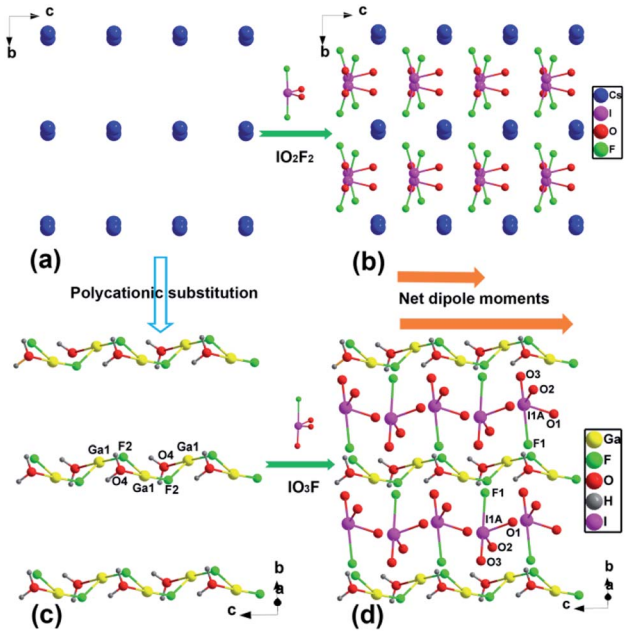

Fig. 1 View of the (a) Cs^+ cations and (b) overall structure of $CsIO_2F_2$, (c) 1D $[GaF(H_2O)]^{2+}$ framework along the *c* axis and (d) 2D $[GaF(H_2O)(IO_3F)]_\infty$ layer on the *bc* plane of $[GaF(H_2O)][IO_3F]$.

–ABAB– sequence along the *a*-axis, stacking into a three-dimensional structure through weak chemical interactions (Fig. 2). The counterpart $CsIO_2F_2$ can be viewed as being made up of Cs^+ cations and embedded IO_2F_2 groups (Fig. 1a and b).[44] Alkali Cs^+ cation is low charged, large, and weakly polarizing, and Cs^+ cations form pure ionic bonds with O/F ions of the IO_2F_2 groups with the average length of 3.17 Å and have a very small impact on the arrangement of the IO_2F_2 groups, which results in a partical offset of the polarity and a relatively low SHG efficiency.[44] In contrast, for $[GaF(H_2O)][IO_3F]$, the main-group Ga^{3+} cation is smaller and more polarizing than the alkali cation, and the Ga–O/F chemical bondings with the average distance of 1.92 Å have a greater degree of covalent characteristic and lower symmetries occur. The catenulate substituent, $[GaF(H_2O)]^{2+}$ framework in $[GaF(H_2O)][IO_3F]$, could

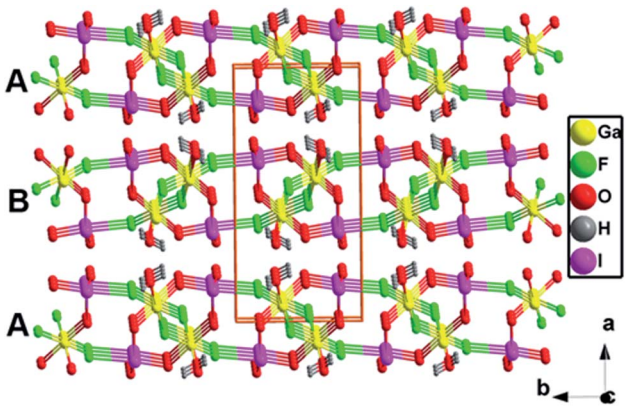

Fig. 2 Three-dimensional structure of $[GaF(H_2O)][IO_3F]$.

effectively guide the favorable arrangement of the polar IO_3F groups, leading to the superposition of the SALPs of I(v) atoms and the polar structure (Fig. 1c and d), which might be highly beneficial to the enhancement of the SHG effect.

The dipole moment calculations of $CsIO_2F_2$ and $[GaF(H_2O)][IO_3F]$ further explain how favorable the alignment of IO_3F groups is in $[GaF(H_2O)][IO_3F]$ (Tables S6, S7† and Fig. 1b, d).[44] Each IO_3F unit in $[GaF(H_2O)][IO_3F]$ has a large local dipole moment of 11.26 D (Debye), comparable to that of IO_2F_2 in $CsIO_2F_2$ (11.96 D) owing to their very similar spatial geometric configurations. At the same time, the extremely orderly arrangement of IO_3F results in an additive net dipole moment of 41.82 D in $[GaF(H_2O)][IO_3F]$, whereas the IO_2F_2 units of $CsIO_2F_2$ counteract a lot with each other, leading to a relatively small value of 33.77 D. Besides, the net dipole moment density of $[GaF(H_2O)][IO_3F]$ is 0.0908 D $Å^{-3}$, which is greatly larger than that of $CsIO_2F_2$ (0.0680 D $Å^{-3}$).

Salt-inclusion compounds with host–guest structure were widely reported in oxide and chalcogenide system, some of which with NCS space group have emerged as a new class of NLO materials, such as $[A_3X][Ga_3PS_8]$ (A = K, Rb; X = Cl, Br) and $Ba_4(BO_3)_3(SiO_4)\cdot Ba_3X$ (X = Cl, Br).[49,57] Generally, the halogen of the halide in salt-inclusion compounds are Br and Cl elements,[47] and F is relatively rare. Notably, the introduction of the most electronegative F^- has been proved to be an effective method to improve the SHG effect and the band gap of oxide NLO materials. Therefore, developing multi-fluorinated salt-inclusion oxides like $[GaF(H_2O)][IO_3F]$ may be a feasible route to isolate NLO crystals with balanced properties. It is worth mentioning that $[GaF(H_2O)][IO_3F]$ with fluorinated IO_3F group is also the first trivalent metal fluoroiodate, and hitherto only alkali-metal and alkaline-earth-metal fluoroiodates have been reported.[58]

The X-ray photoelectron spectroscopy (XPS) analysis results reveal that the molar ratio of Ga : I : O : F on the crystalline powder surface is approximately 1 : 1 : 4 : 2 (Fig. S5†). The solid-state ^{19}F nuclear magnetic resonance (NMR) spectrum displays two peaks with characteristic F chemical shift values of −90.37 and −101.42 ppm, coinciding with the previously reported value,[41] and that these correspond to two different F environments that can exist (Fig. S6†). The relatively wide ^{19}F chemical shift range should ascribe to the stable structure of $[GaF(H_2O)][IO_3F]$ and the low mobility of F^- anions. Elemental analysis (EA) result shows that the percentage of H in the original sample is 0.65%, corresponding to two H atoms of the molecular formula. The thermogravimetric-mass spectrometry (TG-MS) (Fig. S7†) manifests the existence of F^- ions and one coordinating H_2O, and the absence of OH^- group in the molecule. It is worth noting that a small amount of OH^- was released during the thermal process, which can be considered as the ionic fragments of H_2O and is often inevitable during the thermal decomposition.

The IR spectrum reveals that there are several sharp peaks between 881–400 cm^{-1}, and the absorption peaks at 848–741 and 462–433 cm^{-1} could be assigned to the stretching and bending vibrations of I–O bonds, respectively. Besides, the relatively weak peaks at 3424 and 3087 cm^{-1} are associated with the O–H stretching vibration of H_2O units and the absorption peak at 1611 cm^{-1} is caused by the bending vibrations of H_2O groups (Fig. S8†). The ultraviolet-visible-near-infrared (UV-vis-NIR) spectrum indicates that $[GaF(H_2O)][IO_3F]$ has a very short UV absorption cutoff edge of 252 nm and has a wide band gap of 4.34 eV (Fig. S9†), wider than that of AGS (2.65 eV), $AgGaSe_2$ (1.83 eV), and $ZnGeP_2$ (2.0 eV).[59] These spectral analyses show that $[GaF(H_2O)][IO_3F]$ possesses a broad transparent window from near-UV to mid-IR and is a potential candidate for mid-IR optical materials.

Powder SHG measurements revealed that $[GaF(H_2O)][IO_3F]$ exhibits a very large SHG efficiency of 10.0 times that of KDP under 1064 nm incident laser, and it is type-I phase-matchable (Fig. 3). Such an strong SHG signal can be mainly ascribed to the fact that IO_3F groups are arranged in an ordered way and the SALPs of I(v) cations nearly point in the same direction. Compared to the counterpart $CsIO_2F_2$, the SHG response of $[GaF(H_2O)][IO_3F]$ is greatly enhanced. At the same time, its band gap keeps a high value. Consequently, $[GaF(H_2O)][IO_3F]$ possesses extremely balanced physical properties in the reported fluorine iodates (Fig. 4), and these results also illustrate that designing NCS multi-fluorinated salt-inclusion compound is an effective method to regulate the SHG–band gap relationship of NLO crystals.

LDT measurements were performed on powder samples (105–150 μm) together with AGS samples of the same size as the reference. $[GaF(H_2O)][IO_3F]$ displays a giant LDT value of 298.40 MW cm^{-2} (about 140 × AGS (2.13 MW cm^{-2})), which is, to the best of our knowledge, the largest value of the reported iodates SHG crystals, much larger than those of $CsIO_2F_2$ (20 × AGS)[44] and $K_5(W_3O_9F_4)(IO_3)$ (95 × AGS),[38] *etc.* This result could be primarily attributed to the large band gap and salt-inclusion structure of $[GaF(H_2O)][IO_3F]$, and such a high LDT value indicates $[GaF(H_2O)][IO_3F]$ is suitable for high-power laser applications.

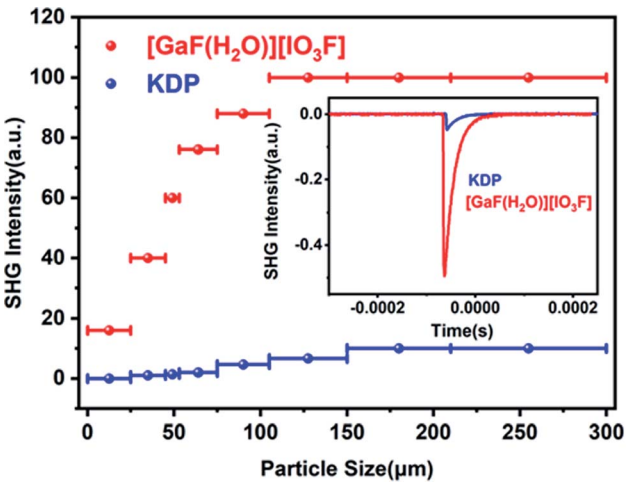

Fig. 3 Diagram of particle size *versus* SHG intensity of $[GaF(H_2O)][IO_3F]$ under laser irradiation at $\lambda = 1064$ nm. Oscilloscope traces of the SHG signals for $[GaF(H_2O)][IO_3F]$ and KDP samples of the same size (150–210 μm) are plotted in the inset.

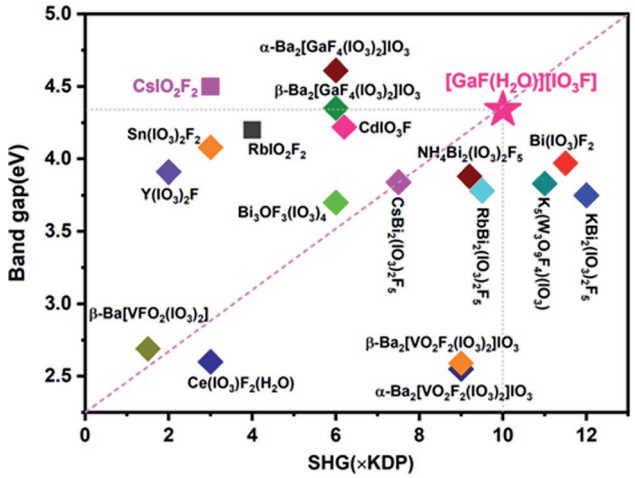

Fig. 4 Comparisons of the SHG effect and the band gap of the reported fluorine iodate NLO materials.

Theoretical calculations with DFT method were performed to deeply study the origin of optical natures of $[GaF(H_2O)][IO_3F]$. Considering the disordered I atom, geometry optimization was applied to the crystallographic structure of $[GaF(H_2O)][IO_3F]$ (ESI, S1† Computational Methods). The calculated band structures (Fig. S10†) reveal an indirect band gap of 4.01 eV for $[GaF(H_2O)][IO_3F]$, slightly smaller than its measured value (4.34 eV), which was caused by the discontinuity of the exchange–correlation functional.[60] Hence, a scissor value of 0.33 eV was adopted to compute the optical properties of $[GaF(H_2O)][IO_3F]$. The total and partial density of states of $[GaF(H_2O)][IO_3F]$ (Fig. S11†) display that the electronic states at the top of the valence band (VB) are mainly F 2p and O 2p orbitals, while the bottom of conduction band (CB) is dominated by I 5p and O 2p orbitals. The distribution of density of states indicates that the electron transition activity near the forbidden band is mainly determined by the electronic states of iodine, oxygen, and fluorine atoms.

Inorganic crystals with 2D layered structure possibly possess large optical anisotropy and great birefringence.[61] Linear optical calculations disclosed that the birefringence of $[GaF(H_2O)][IO_3F]$ is 0.142 at 1064 nm and 0.166 at 532 nm, fully meeting the requirement of phase matching process (Fig. S12†). The refractive indices show that $[GaF(H_2O)][IO_3F]$ is a positive biaxial birefringent crystal as the value of $n_x - n_y$ is larger than $n_y - n_z$.

Based on the structural and Kleinman's symmetry, the second-order NLO coefficient study gave a maximum tensor of 3.94 pm V^{-1} (d_{32}) for $[GaF(H_2O)][IO_3F]$, which is relatively close to the experimental SHG effect of 10 × KDP (d_{36} (KDP at 1064 nm) = 0.39 pm V^{-1}). The SHG density diagram of d_{32} (Fig. S13†) clearly describes the contributions of different atoms and functional building blocks. In the VB, the 2p nonbonding orbitals of all O and F atoms play a crucial role in contributing the SHG effect. As for the CB, the chief contributor is O 2p and F 2p electronic states of $[IO_3F]$ units, and the contribution of $[GaF(H_2O)]$ groups is almost negligible. Combining the SHG contribution densities of the VB and CB, the accurate contribution percentages of $[IO_3F]^{2-}$ and $[GaF(H_2O)]^{2+}$ units are 71.06% and 28.24%, respectively, which means that the substitution of Cs^+ with $[GaF(H_2O)]^{2+}$ polycation plays the critical role in improving NLO coefficient.

Conclusions

In conclusion, a new fluoroiodate $[GaF(H_2O)][IO_3F]$ based on $CsIO_2F_2$ was successfully obtained through an ingenious anisotropic polycation substitution approach. The compound features a polar layered salt-inclusion structure and the catenulate $[GaF(H_2O)]^{2+}$ polycation framework not only acts as a template for the favourable arrangement of the polar $[IO_3F]^{2-}$ groups but also contributes to the NLO coefficient. In comparison with the parent compound $CsIO_2F_2$ (3 × KDP, 4.5 eV), the SHG effect of $[GaF(H_2O)][IO_3F]$ increase to 10KDP and a wide band gap of 4.34 eV remains. Furthermore, $[GaF(H_2O)][IO_3F]$ has a broad transparent spectral region from near-UV to mid-IR and the largest LDT of 140 times that of AGS of the reported iodates. These superior performances indicate that $[GaF(H_2O)][IO_3F]$ is a promising mid-IR NLO material. This work suggests that anisotropic polycation substitution is a feasible route to optimize NLO properties and isolate promising SHG crystals. Therefore, the discovery of $[GaF(H_2O)][IO_3F]$ is of great significance for the development of inorganic functional material and NLO optics.

Data availability

All of the related experimental and computational data are provided in the electronic supplementary information.

Author contributions

Q. M. H. synthesized the compound and performed most experiments. C. L. H. performed the optical theoretical calculations. B. X. L. performed LDT measurements. Q. M. H. and B. P. Y. analyzed the X-ray diffraction data and all physical tests, and wrote the manuscript. All authors provided input on the manuscript.

Conflicts of interest

The authors declare no competing financial interest.

Acknowledgements

This work was supported by the National Natural Science Foundation of China (Grant nos. 21975256, 22031009 and 21921001) and the Strategic Priority Research Program of Chinese Academy of Sciences (Grant no. XDB20000000).

Notes and references

1 C. T. Chen and G. Z. Liu, *Annu. Rev. Mater. Sci.*, 1986, **16**, 203–243.

2 P. S. Halasyamani and K. R. Poeppelmeier, *Chem. Mater.*, 1998, **10**, 2753–2769.
3 T. T. Tran, H. Yu, J. M. Rondinelli, K. R. Poeppelmeier and P. S. Halasyamani, *Chem. Mater.*, 2016, **28**, 5238–5258.
4 K. M. Ok, *Acc. Chem. Res.*, 2016, **49**, 2774–2785.
5 G. Zou and K. M. Ok, *Chem. Sci.*, 2020, **11**, 5404–5409.
6 X. Liu, P. Gong, Y. Yang, G. Song and Z. Lin, *Coord. Chem. Rev.*, 2019, **400**, 213045.
7 M. Mutailipu, M. Zhang, H. Wu, Z. Yang, Y. Shen, J. Sun and S. Pan, *Nat. Commun.*, 2018, **9**, 3089.
8 M. Mutailipu, M. Zhang, Z. Yang and S. Pan, *Acc. Chem. Res.*, 2019, **52**, 791–801.
9 X. Lian, W.-D. Yao, W. Liu, R.-L. Tang and S.-P. Guo, *Inorg. Chem.*, 2021, **60**, 19–23.
10 M. Mutailipu, K. R. Poeppelmeier and S. Pan, *Chem. Rev.*, 2021, **121**, 1130–1202.
11 H. Fan, C. Lin, K. Chen, G. Peng, B. Li, G. Zhang, X. Long and N. Ye, *Angew. Chem., Int. Ed.*, 2020, **59**, 5268–5272.
12 Q. Wu, H. Liu, F. Jiang, L. Kang, L. Yang, Z. Lin, Z. Hu, X. Chen, X. Meng and J. Qin, *Chem. Mater.*, 2016, **28**, 1413–1418.
13 R. Wang, F. Liang, F. Wang, Y. Guo, X. Zhang, Y. Xiao, K. Bu, Z. Lin, J. Yao, T. Zhai and F. Huang, *Angew. Chem., Int. Ed.*, 2019, **58**, 8078–8081.
14 B. N. Carnio, K. T. Zawilski, P. G. Schunemann and A. Y. Elezzabi, *Opt. Lett.*, 2019, **44**, 2867–2869.
15 V. Petrov, F. Rotermund and F. Noack, *Opt. Lett.*, 1999, **24**, 414–416.
16 A. O. Okorogu, S. B. Mirov, W. Lee, D. I. Crouthamel, A. Y. Dergachev, K. L. Vodopyanov, N. Jenkins and V. V. Badikov, *Opt. Commun.*, 1998, **155**, 307–312.
17 W. Wang, D. Mei, F. Liang, J. Zhao, Y. Wu and Z. Lin, *Coord. Chem. Rev.*, 2020, **421**, 213444.
18 S. P. Guo, Y. Chi and H. G. Xue, *Angew. Chem., Int. Ed.*, 2018, **57**, 11540–11543.
19 S. P. Guo, X. Cheng, Z. D. Sun, Y. Chi, B. W. Liu, X. M. Jiang, S. F. Li, H. G. Xue, S. Deng, V. Duppel, J. Kohler and G. C. Guo, *Angew. Chem., Int. Ed.*, 2019, **58**, 8087–8091.
20 M.-M. Chen, H.-G. Xue and S.-P. Guo, *Coord. Chem. Rev.*, 2018, **368**, 115–133.
21 R. E. Sykora, K. M. Ok, P. S. Halasyamani and T. E. Albrecht-Schmitt, *J. Am. Chem. Soc.*, 2002, **124**, 1951–1957.
22 C. F. Sun, C. L. Hu, X. Xu, B. P. Yang and J. G. Mao, *J. Am. Chem. Soc.*, 2011, **133**, 5561–5572.
23 Y. Suffren and I. Gautier-Luneau, *Eur. J. Inorg. Chem.*, 2012, **2012**, 4264–4267.
24 C. F. Sun, C. L. Hu and J. G. Mao, *Chem. Commun.*, 2012, **48**, 4220–4222.
25 Y. Huang, X. Meng, P. Gong, L. Yang, Z. Lin, X. Chen and J. Qin, *J. Mater. Chem. C*, 2014, **2**, 4057–4062.
26 Y. Li, G. Han, H. Yu, H. Li, Z. Yang and S. Pan, *Chem. Mater.*, 2019, **31**, 2992–3000.
27 C. F. Sun, C. L. Hu, X. Xu, J. B. Ling, T. Hu, F. Kong, X. F. Long and J. G. Mao, *J. Am. Chem. Soc.*, 2009, **131**, 9486–9487.
28 H. Y. Chang, S. H. Kim, K. M. Ok and P. S. Halasyamani, *J. Am. Chem. Soc.*, 2009, **131**, 6865–6873.
29 Y. H. Kim, T. T. Tran, P. S. Halasyamani and K. M. Ok, *Inorg. Chem. Front.*, 2015, **2**, 361–368.
30 F.-F. Mao, C.-L. Hu, J. Chen and J.-G. Mao, *Chem. Mater.*, 2018, **30**, 2443–2452.
31 Y. J. Jia, Y. G. Chen, Y. Guo, X. F. Guan, C. Li, B. Li, M. M. Liu and X. M. Zhang, *Angew. Chem., Int. Ed.*, 2019, **58**, 17194–17198.
32 K. M. Ok and P. S. Halasyamani, *Angew. Chem., Int. Ed.*, 2004, **43**, 5489–5491.
33 D. Phanon and I. Gautier-Luneau, *Angew. Chem., Int. Ed.*, 2007, **46**, 8488–8491.
34 X. Xu, C.-L. Hu, B.-X. Li, B.-P. Yang and J.-G. Mao, *Chem. Mater.*, 2014, **26**, 3219–3230.
35 J. Chen, C. L. Hu, F. F. Mao, B. P. Yang, X. H. Zhang and J. G. Mao, *Angew. Chem., Int. Ed.*, 2019, **58**, 11666–11669.
36 Q.-M. Huang, C.-L. Hu, B.-P. Yang, R.-L. Tang, J. Chen, Z. Fang, B. Li and J.-G. Mao, *Chem. Mater.*, 2020, **32**, 6780–6787.
37 S. D. Nguyen, J. Yeon, S.-H. Kim and P. S. Halasyamani, *J. Am. Chem. Soc.*, 2011, **133**, 12422–12425.
38 C. Wu, L. Lin, X. Jiang, Z. Lin, Z. Huang, M. G. Humphrey, P. S. Halasyamani and C. Zhang, *Chem. Mater.*, 2019, **31**, 10100–10108.
39 Y. J. Jia, Y. G. Chen, T. Wang, Y. Guo, X. F. Guan and X. M. Zhang, *Dalton Trans.*, 2019, **48**, 10320–10326.
40 F. You, F. Liang, Q. Huang, Z. Hu, Y. Wu and Z. Lin, *J. Am. Chem. Soc.*, 2019, **141**, 748–752.
41 F. F. Mao, C. L. Hu, X. Xu, D. Yan, B. P. Yang and J. G. Mao, *Angew. Chem., Int. Ed.*, 2017, **56**, 2151–2155.
42 H. Liu, Q. Wu, X. Jiang, Z. Lin, X. Meng, X. Chen and J. Qin, *Angew. Chem., Int. Ed.*, 2017, **56**, 9492–9496.
43 M. Zhang, X. Su, M. Mutailipu, Z. Yang and S. Pan, *Chem. Mater.*, 2017, **29**, 945–949.
44 M. Zhang, C. Hu, T. Abudouwufu, Z. Yang and S. Pan, *Chem. Mater.*, 2018, **30**, 1136–1145.
45 J. Chen, C. L. Hu, F. F. Mao, J. H. Feng and J. G. Mao, *Angew. Chem., Int. Ed.*, 2019, **58**, 2098–2102.
46 H. Yu, M. L. Nisbet and K. R. Poeppelmeier, *J. Am. Chem. Soc.*, 2018, **140**, 8868–8876.
47 Q.-G. Yue, W.-B. Wei, H. Chen, X.-T. Wu, H. Lin and Q.-L. Zhu, *Dalton Trans.*, 2020, **49**, 14338–14343.
48 B. W. Liu, X. M. Jiang, H. Y. Zeng and G. C. Guo, *J. Am. Chem. Soc.*, 2020, **142**, 10641–10645.
49 B.-W. Liu, H.-Y. Zeng, X.-M. Jiang, G.-E. Wang, S.-F. Li, L. Xu and G.-C. Guo, *Chem. Sci.*, 2016, **7**, 6273–6277.
50 P. Yu, L.-J. Zhou and L. Chen, *J. Am. Chem. Soc.*, 2012, **134**, 2227–2235.
51 J. P. West and S.-J. Hwu, *J. Solid State Chem.*, 2012, **195**, 101–107.
52 H. Lin, W.-B. Wei, H. Chen, X.-T. Wu and Q.-L. Zhu, *Coord. Chem. Rev.*, 2020, **406**, 213150.
53 B. W. Liu, X. M. Jiang, B. X. Li, H. Y. Zeng and G. C. Guo, *Angew. Chem., Int. Ed.*, 2019, **59**, 4856–4859.
54 X. A. Chen, H. P. Xue, X. A. Chang, H. G. Zang and W. Q. Xiao, *Acta Crystallogr., Sect. C: Cryst. Struct. Commun.*, 2005, **61**, I109–I110.

55 G. Park and K. M. Ok, *Inorg. Chem. Front.*, 2020, **7**, 4469–4476.
56 N. E. Brese and M. Okeeffe, *Acta Crystallogr., Sect. B: Struct. Sci.*, 1991, **47**, 192–197.
57 X. Lin, F. Zhang, S. Pan, H. Yu, F. Zhang, X. Dong, S. Han, L. Dong, C. Bai and Z. Wang, *J. Mater. Chem. C*, 2014, **2**, 4257.
58 M. Gai, T. Tong, Y. Wang, Z. Yang and S. Pan, *Chem. Mater.*, 2020, **32**, 5723–5728.
59 B. Tell and H. M. Kasper, *Phys. Rev. B*, 1971, **4**, 4455–4459.
60 S. Mattsson and B. Paulus, *J. Comput. Chem.*, 2019, **40**, 1190–1197.
61 C. Wu, G. Yang, M. G. Humphrey and C. Zhang, *Coord. Chem. Rev.*, 2018, **375**, 459–488.